

Supplemental information

**4-Phenylbutyrate restores
localization and membrane repair
to human dysferlin mutations**

Kana Tominaga, Naomi Tominaga, Eric O. Williams, Laura Rufibach, Verena Schöwel, Simone Spuler, Mohan Viswanathan, and Leonard P. Guarente

Supplementary Figures

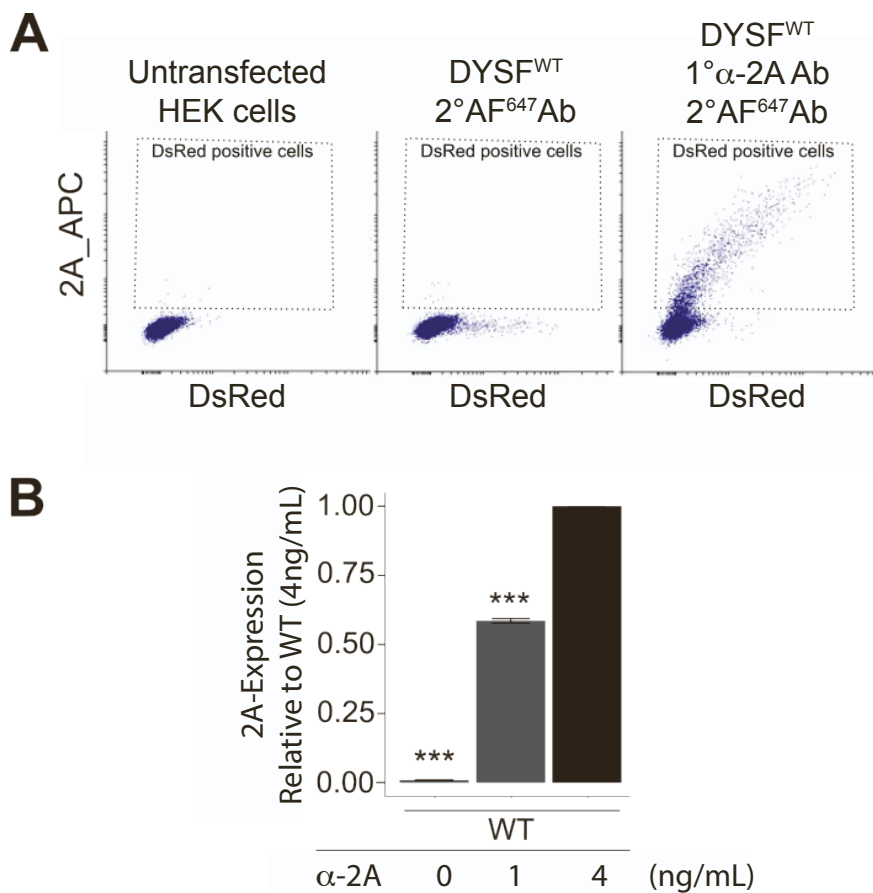


Fig. S1. Validation of α -2A Ab detection of PM-localized DYSF in 2A assay, related to Figure 1. (A) Flow cytometry dot plots analyzing DYSF-2A detection in non-transfected HEK cells and HEK cells transiently transfected with DYSF^{WT}. Cells expressing DYSF^{WT} were hybridized with α -2A 1° Ab and Alexa Fluor 647 conjugated-IgG 2°Ab as labelled. The flow cytometer fluorescence wavelength detector was set for allophycocyanin (APC), which detects Alexa Fluor 647. (B) Determination of α -2A 1° Ab range of detection of PM-localized DYSF^{WT} in HEK cells ($n = 3$). *** $p < 0.001$ indicates difference between 4 ng/ml and 0 or 1 ng/ml.

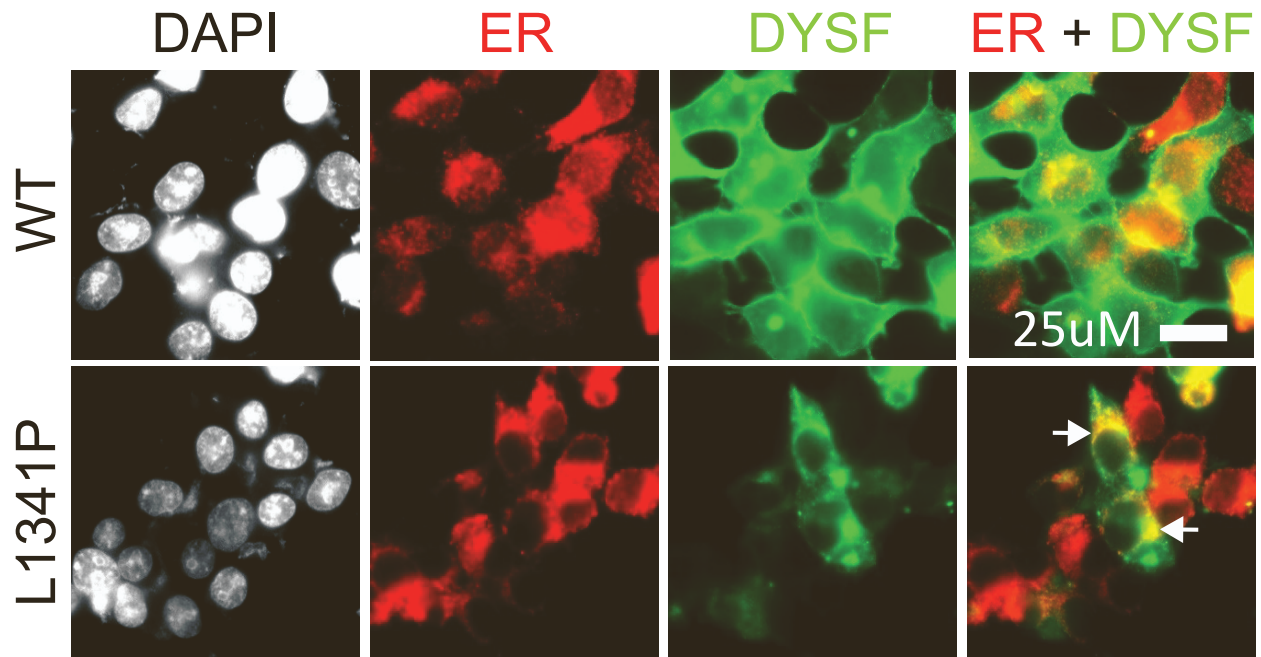


Fig. S2. Immunofluorescence images localizing DYSF^{PMMs} expressed in HEK293T cells, related to Figure 1. 48-hrs post transfection HEK293T cells expressing DYSF^{L1341P} were FACS sorted for DsRed, cultured, fixed, and hybridized with the Hamlet α -DYSF 1° Ab (green) and the α -Calreticulin 1° Ab (red) to identify the endoplasmic reticulum (ER). Arrows point to perinuclear areas where DYSF^{L1341P} localization is coincident with ER. Scale bar: 25 microns.

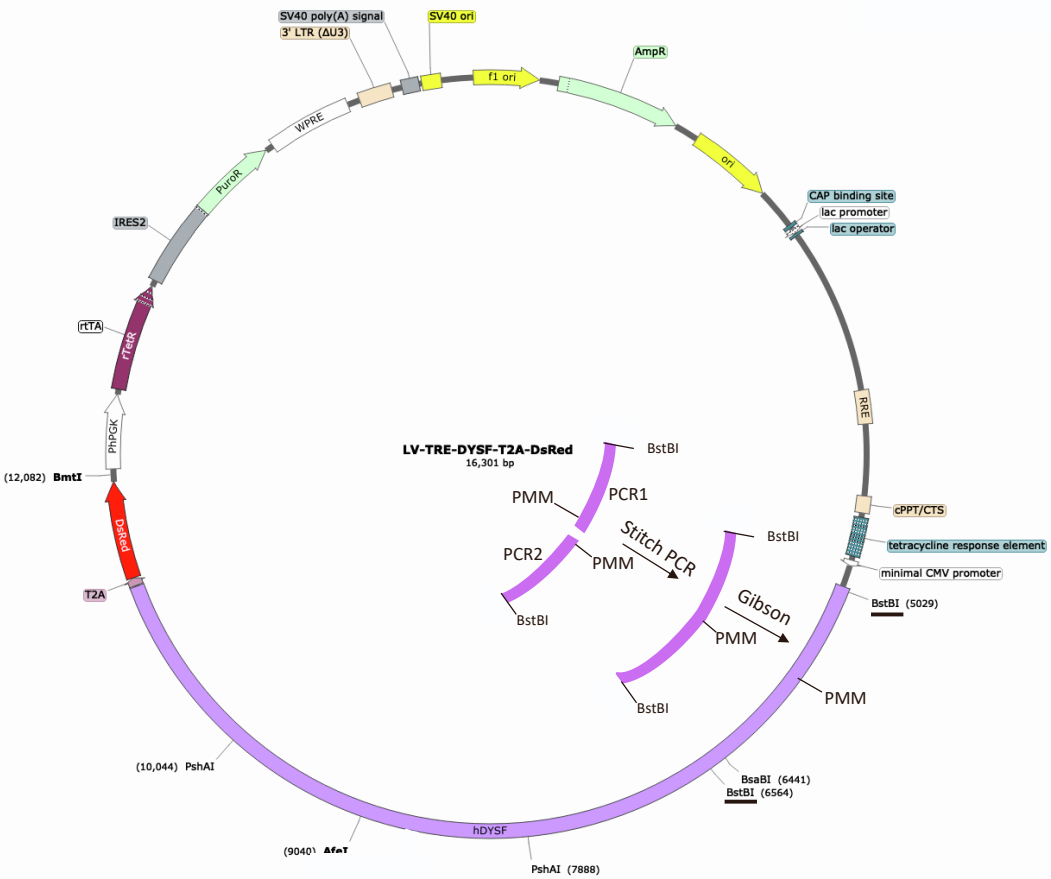


Fig. S3. PCR stitching and Gibson cloning scheme for introduction of DYSF PMMs into LV-TRE-DYSF-T2A-DsRed, related to Figure 1 and Table S1. A DYSF^{PMM}-containing PCR product was produced by PCR stitching two separate PCR products, PCR1 and PCR2, each with overlapping regions of homology containing the PMM introduced in the PCR oligonucleotides. This product was then used for Gibson assembly into linearized LV-TRE-DYSF-T2A-DsRed using the appropriate restriction enzymes listed in Table S1. Example shown is for Gibson assembly of PCR products containing DYSF^{PMMs} between BstBI sites, similar products were generated for other regions of DYSF.

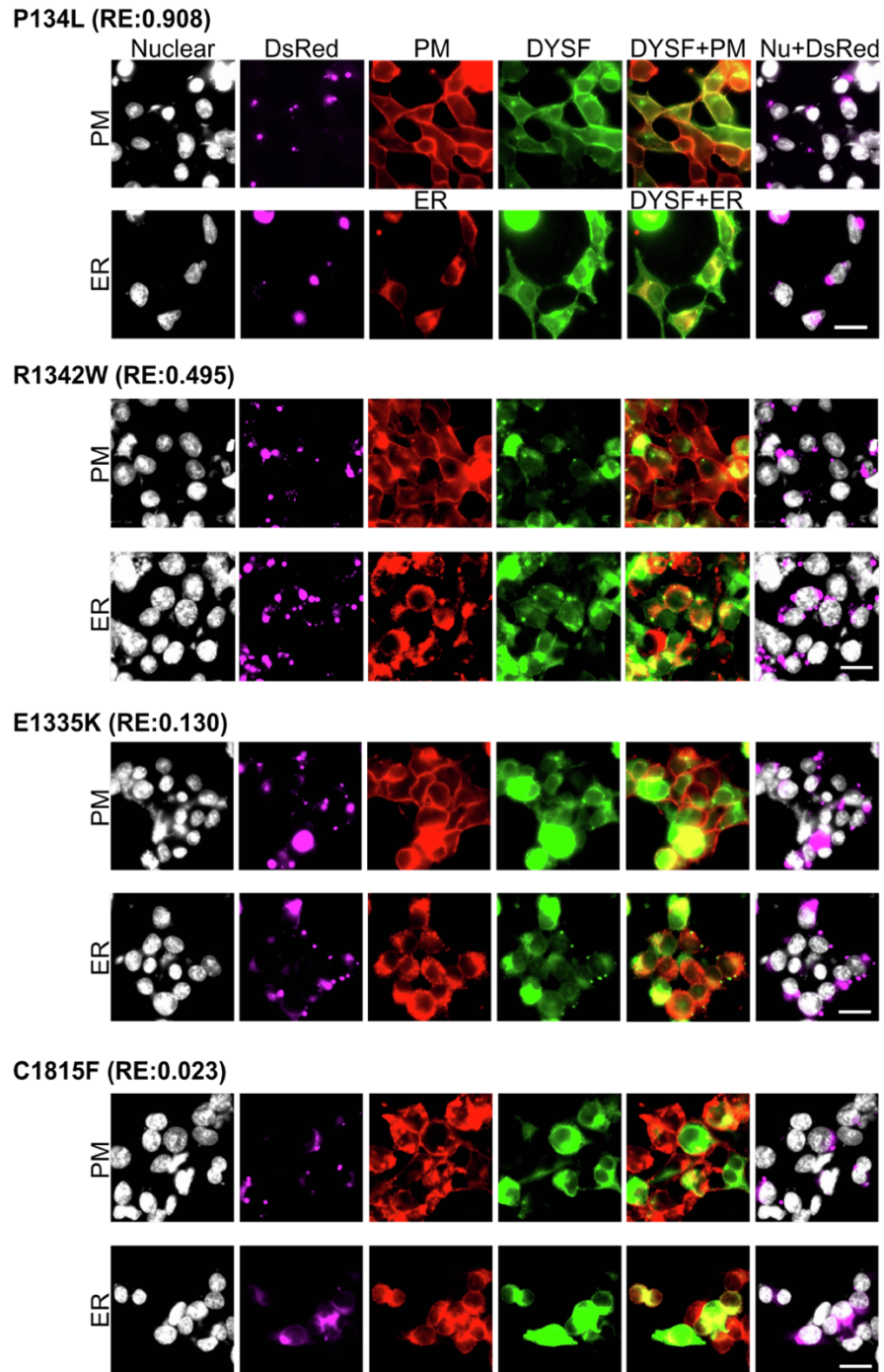


Fig. S4. Immunofluorescence images showing PM localization of DYSF in HEK cells expressing DYSF^{P134L}, DYSF^{R1342W}, DYSF^{E1335K}, or DYSF^{C1815F}, related to Figure 2. HEK cells were transiently transfected with a DYSF^{PMM} expression construct, cultured for 48-hrs, and sorted for DsRed positive cells. Following 24-hrs of culture, cells were processed for ICC with α -DYSF Ab (green), α -sodium potassium ATPase Ab PM (red) and α -calreticulin Ab ER (red) to aid in identification of these organelles, as well as DAPI nuclear marker (Nu). RE, Relative expression to WT. Scale bar: 25 microns.

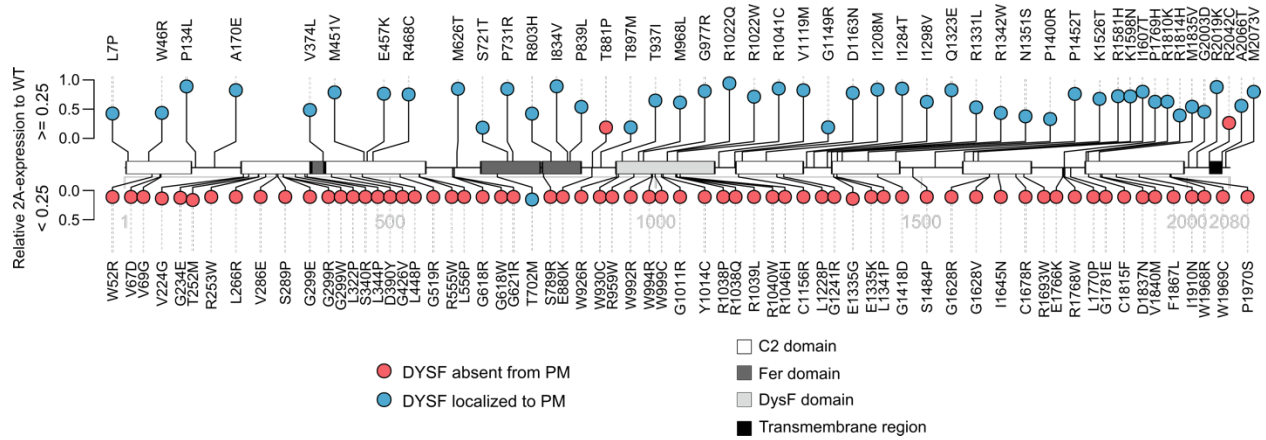


Fig. S5. 2A-assay and ICC results for 113 DYSF^{PMMs} expressed in HEK cells: DYSF gene lollipop, related to Figure 2 and Table S1. Plotted on the y-axis (DYSF protein domains annotated) are the average 2A-assay values ($n=3$) of PM-localized DYSF^{PMM} relative to DYSF^{WT}. Values are directionally plotted based on 25% threshold of PM-localization in 2A-assay with PMMs below threshold plotted below the x-axis in red and PMMs above threshold plotted above the x-axis in blue. Lollipop was created using R Bioconductor.

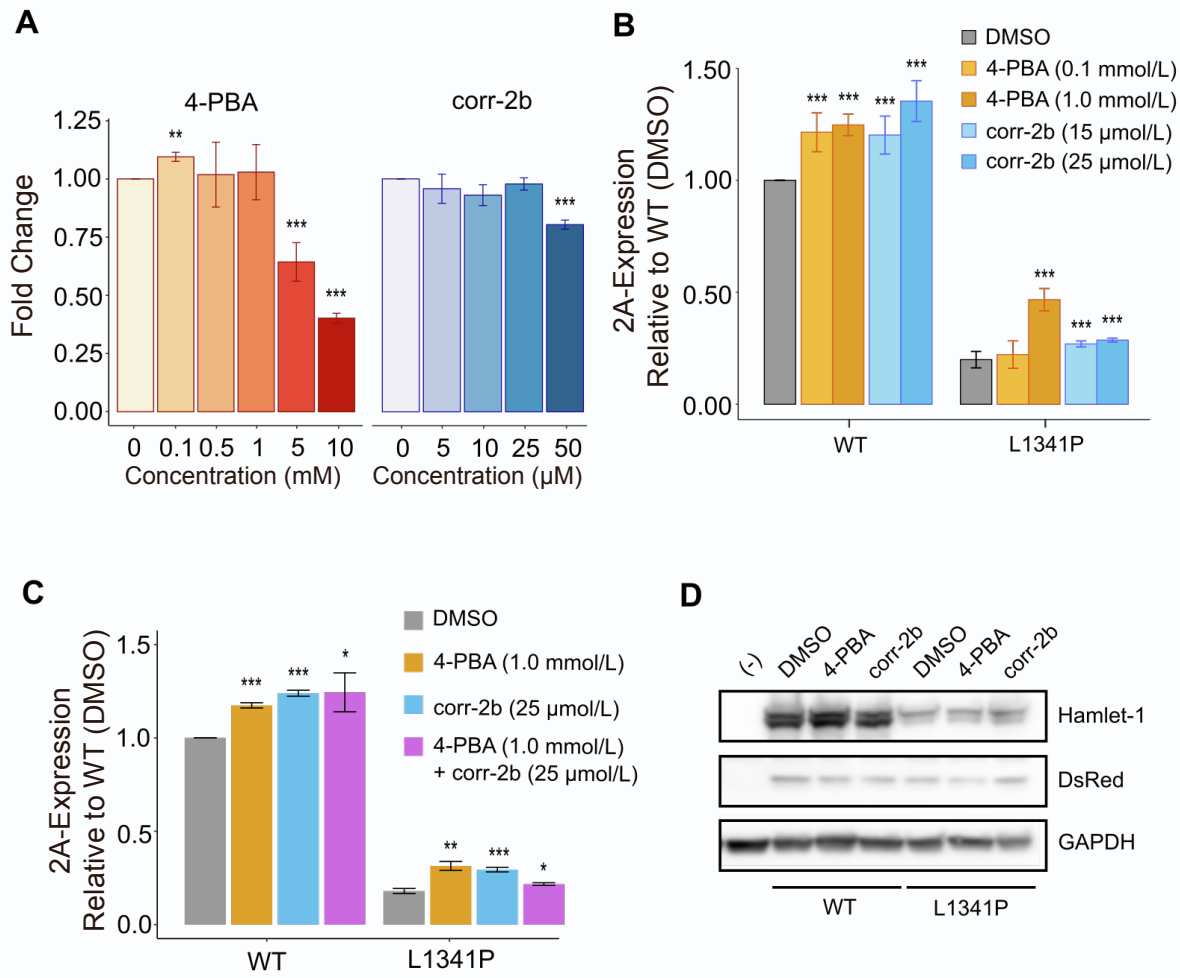


Fig. S6. Evaluation of 4-PBA and corr-2b efficacy, related to Figure 3. (A) Cell proliferation assays for HEK cells treated with 4-PBA or corr-2b compared to DMSO alone for 24-hrs demonstrates that 4-PBA and corr-2b prevent cell proliferation at concentrations greater than 1mM and 25 μ M, respectively (B) Dose response of 4-PBA and corr-2b in 2A-assays with DYSF^{L1341P} shows optimal effect of 4-PBA and corr-2b are at 1mM and 25 μ M, respectively. All values are normalized to cells expressing DYSF^{WT} treated with DMSO. (C) Combination of 4-PBA and corr-2b treatment shows no additivity compared with a single treatment in 2A-assay response relative to DMSO treated DYSF^{WT}. (D) Effect of drug treatments on DYSF expression in HEK cells transiently transfected with DYSF^{WT} or DYSF^{L1341P}. HEK cells expressing DYSF^{WT} or DYSF^{L1341P} were incubated with either DMSO (0.1%), 4-PBA (1 mM), corr-2b (25 μ M) for 24-hrs and subject to western blot of total protein lysates from each cell line under each treatment. Non-transfected HEK cells were used as negative control. Membranes were hybridized with α -DYSF(Hamlet) Ab, and α -DsRed 1° Ab and α -GAPDH 1° Ab as loading control. *p < 0.05, **p<0,01, ***p<0.001, relative to untreated or DMSO control.

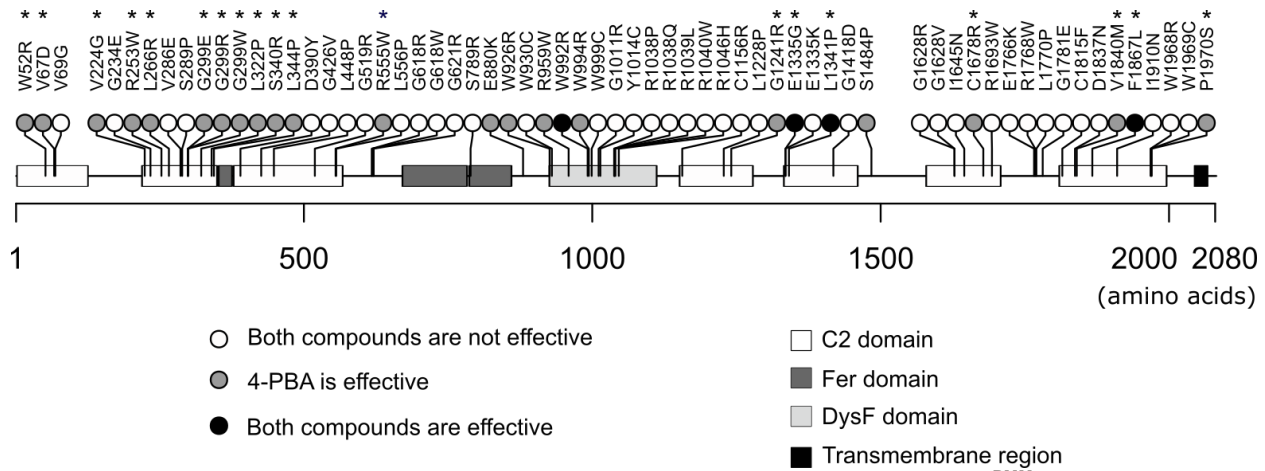


Fig. S7. 4-PBA is highly effective in restoring PM-localization to various DYSF^{PMMs} across the various domains, related to Figure 3. Lollipop showing effect of 4-PBA or corr-2b treatment on 64 missense mutations across the DYSF cDNA. Asterisks show nineteen mutations in C2 domains rescued by 4-PBA. Lollipop was created using R Bioconductor.

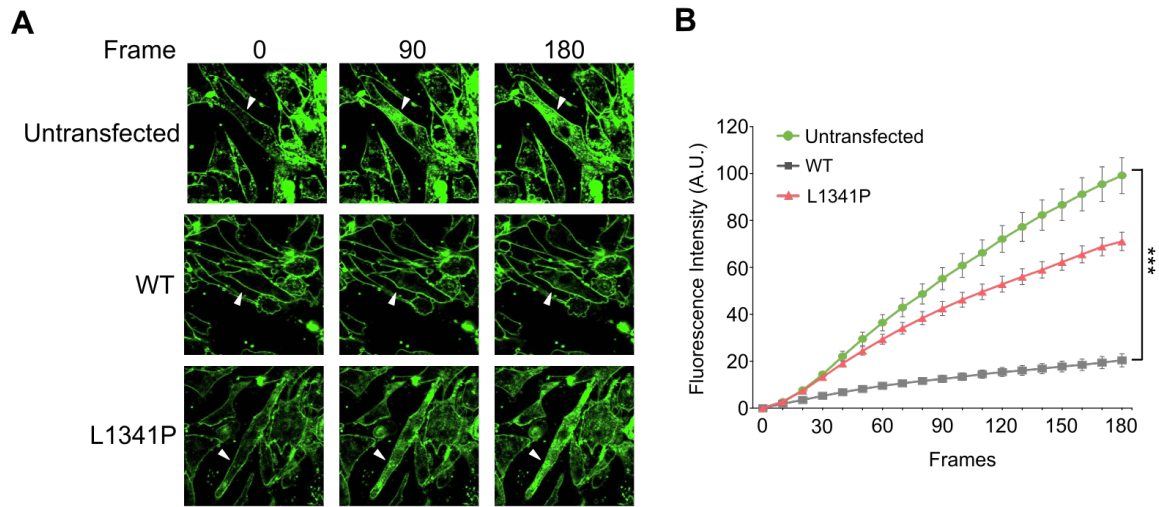


Fig. S8. Membrane repair in GREG cell derived myotubes, related to Figures 2, 4A, 4B, and S9. Dysferlin deficient GREG myoblasts were transfected with DYSF^{WT} or DYSF^{L1341P} expression vectors, cultured, and subsequently sorted for DsRed positive myoblasts. Sorted cells, as well as non-transfected GREG cells, were plated in chambered cover glass in differentiation media and cultured into myotubes. Myotubes were laser (405nm) wounded in the presence of calcium and FM1-43 dye (green). Untransfected and DYSF^{L1341P} transfected myotubes failed to repair laser induced membrane damage, while myotubes expressing DYSF^{WT} rapidly repaired the breach. **(A)** Three image frames are presented for each sample; the first image is at the time of wounding, the second in the middle of repair, and the third at the end of repair. Arrowheads show the site of injury. **(B)** Repair kinetics of non-transfected GREG cells ($n = 13$), and GREG cells expressing DYSF^{WT} ($n = 19$) or DYSF^{L1341P} ($n = 23$) as measured by FM1-43 dye influx into the myotube injury site. Data area means +/- S. E. M. ***p<0.001

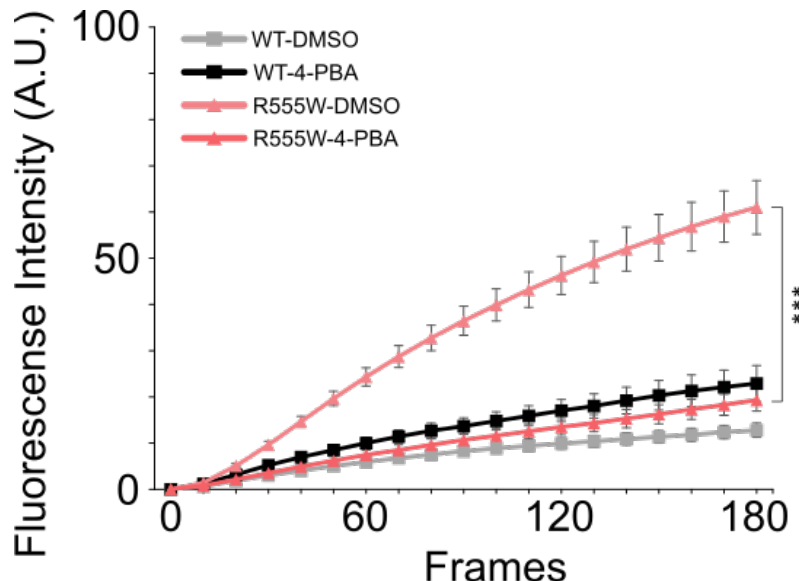


Fig. S9. 4-PBA treatment restores membrane repair to GREG myotubes expressing DYSF^{R555W}, related to Figures 3A, 4A, and 4B. Kinetic analysis of FM1-43 dye influx in transfected dysferlin deficient GREG myotubes after laser membrane damage. Number of transfected and treated myotubes assayed: DYSF^{WT}(DMSO) (n = 10), DYSF^{WT} (4-PBA) (n = 10), DYSF^{R555W}(DMSO) (n = 15), or DYSF^{R555W} (4-PBA) (n = 13). Data are means ± S.E.M., ***p<0.001.

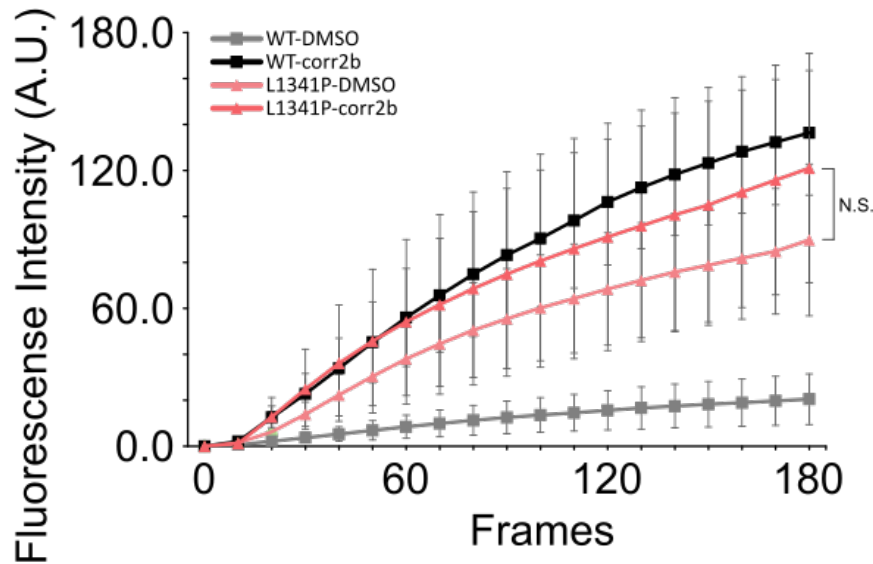


Fig. S10. corr-2b treatment of GREG myotubes prevents membrane repair in the presence of DYSF^{WT} and sensitizes non-transfected GREG myotubes to damage, related to Figure 3. Kinetic analysis of FM1-43 dye influx in dysferlin deficient GREG myotubes after laser damage (405nm). Number of transfected and treated myotubes assayed: DYSF^{WT}(DMSO) (n = 12), DYSF^{WT} (corr-2b) (n = 6), DYSF^{L1341P} (DMSO) (n = 9), or DYSF^{L1341P} (corr-2b) (n = 7). N.S.; not significant. Plotted values are means ± S.E.M.

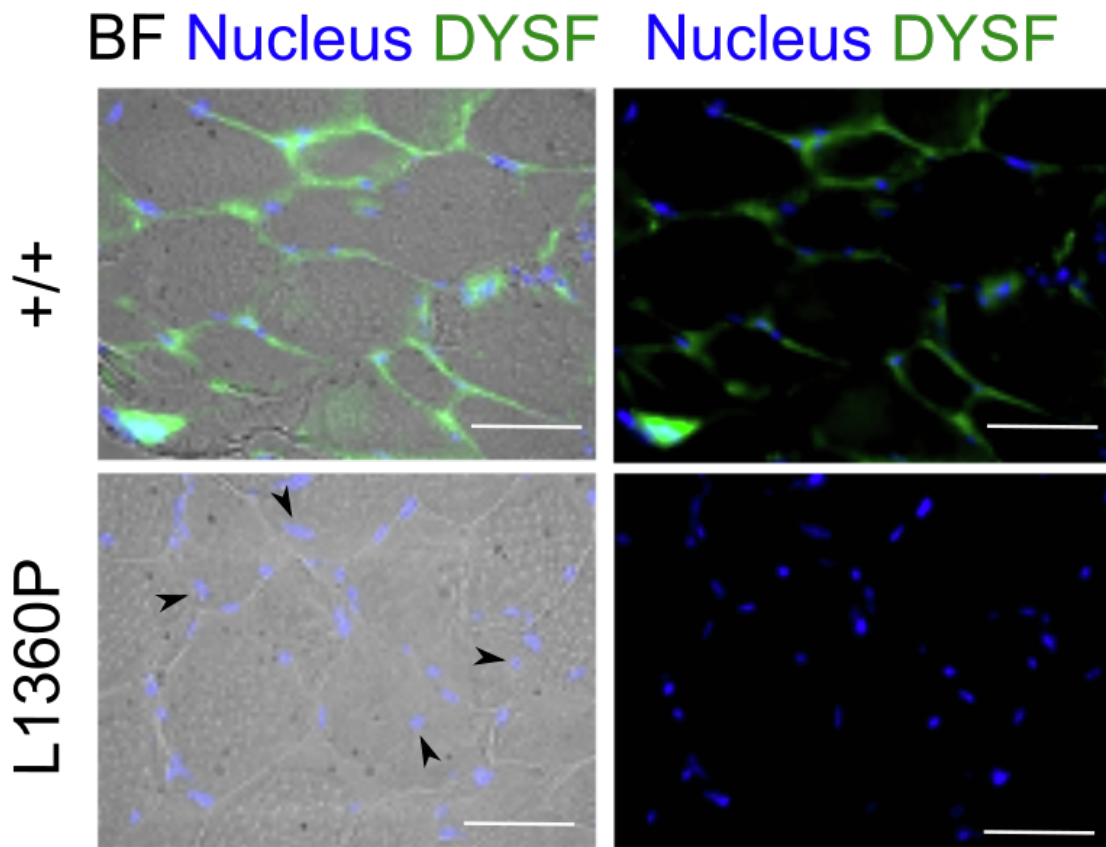
A

Fig. S11. Histological analysis of EDL muscle cross-section from MMex38 $\text{DYSF}^{\text{L1360P}}$ mice show hallmarks of dysferlinopathy, related to Figures 4C, 4D, and 4E. Brightfield and immunofluorescence images of EDL muscle fibers obtained from C57BL/6NJ (20-month, male) or MMex38 (20-month, male) mice using Romeo α -DYSF 1° Ab with DAPI nuclear staining shows that sarcolemma localization of DYSF seen in control animals is absent in MMex38, as well as central nuclei (arrows) within myofibers in MMex38 mice, indicative of dystrophic muscle. Scale bar: 50 microns.

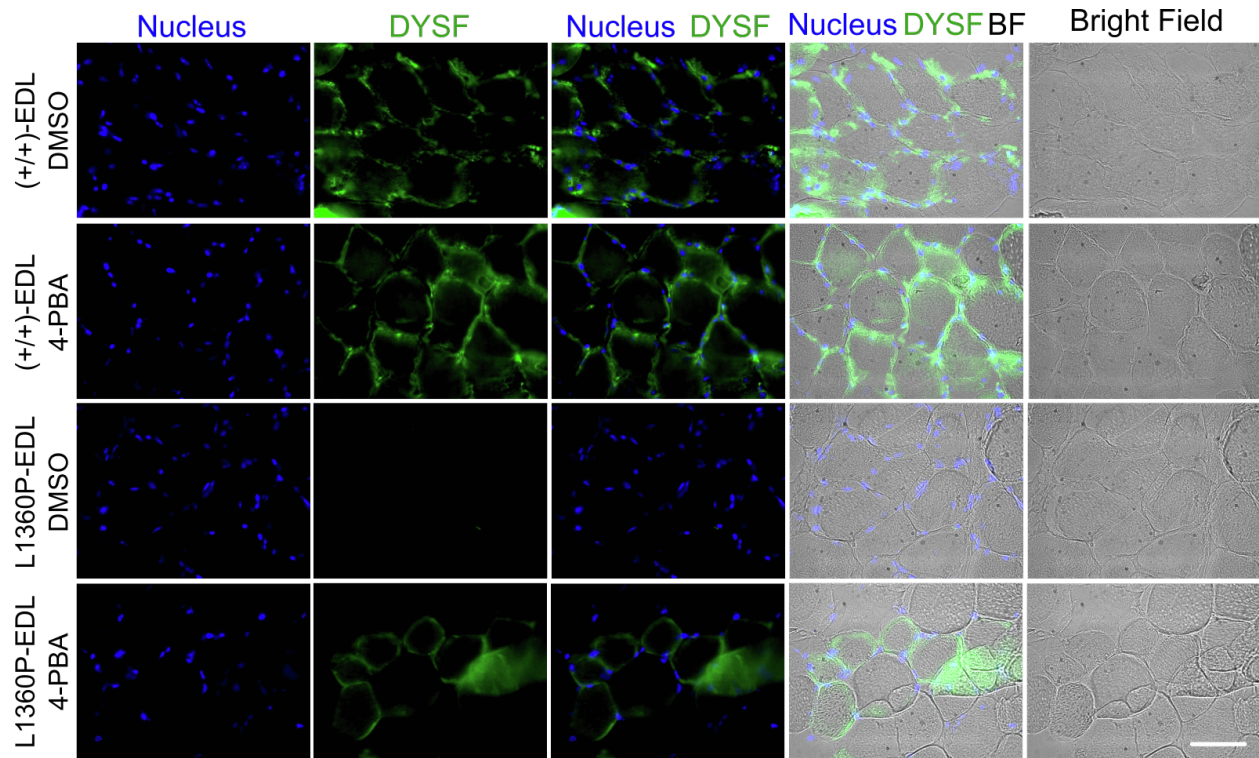


Fig. S12. Ex vivo treatment of MMex38 mice EDL with 4-PBA rescues DYSF sarcolemma expression, related to Figure 4. EDL muscle isolated from male C57BL6/NJ (+/+) and MMex38 mice and cultured in either vehicle (0.1% DMSO) or 4-PBA (1mM) for 24-hrs. Fresh frozen cross-sections of the treated EDL muscles were subsequently prepared for histological analysis. DAPI staining was performed for nuclear localization and DYSF staining was done using Hamlet α -DYSF 1^o Ab and Alexa 647 α -mouse fluorescent 2^o Ab. Images were all taken at the same exposure time and magnification. Scale bar: 50 microns. Brightfield images and overlays show myofiber structures in the absence of any staining. Muscle cross section of EDL muscle from untreated MMex38 mice show no DYSF expression, while similar cross sections from 4-PBA treated MMex38 mice, shows increased DYSF^{L1360P} expression and staining of myofiber sarcolemma.

Supplemental Tables

Table S1:DYSF^{PMMs} Engineering and HEK Cell Results

Table S1. List of DYSF^{PMMs} used in this study, related to Figure 1, Figure 2, and Figure S3. Included are results of 2A-assays in HEK cells, ICC results of DYSF localization in HEK cells, and oligonucleotides used for the construction of DYSF^{PMMs} expression vectors.

Table S1:DYSF^{PMMs} Engineering and HEK Cell Results (continued)

Table S1 continued. List of DYSF^{PMMs} used in this study, related to Figure 1, Figure 2, and Figure S3. Included are results of 2A-assays in HEK cells, ICC results of DYSF localization in HEK cells, and oligonucleotides used for the construction of DYSF^{PMMs} expression vectors.

Table S2: DYSF^{PMMs} Present in the Homozygous State in Individuals from the Dyferlin Registry

DYSF Missense Mutation (36 Variants)	# of patients (90 Total)	2A-Expression Value	Exon Skipping
R2019K	2	0.90	Yes
R1041C	1	0.88	
G977R	1	0.83	
I1607T	3	0.83	
P1452T	1	0.79	
K1526T	1	0.72	
R1810K	1	0.67	Yes
P1769H	1	0.67	
R1331L	2	0.58	
R2042C	4	0.34	
T252M	1	0.25	
V224G	1	0.22	
W926R	1	0.19	
R1693W	3	0.18	
C1156R	1	0.16	
V69G	6	0.16	
S340R	2	0.16	
G1418D	6	0.16	
V67D	1	0.15	
W52R	1	0.14	
R253W	2	0.13	
R959W	2	0.13	
R1038Q	2	0.11	
Y1014C	11	0.10	
I1645N	1	0.10	
G299W	1	0.10	
R1768W	2	0.09	
G618R	2	0.09	
R555W	6	0.09	
L556P	1	0.09	
G519R	2	0.09	
R1046H	10	0.09	
L1341P	5	0.08	
G1628R	1	0.05	
W1968R	1	0.03	
W1969C	1	0.03	
# of variants			
2A < 0.25 (No PM localization)			26 (72%)
Exon Skipping Mutants, 2A > 0.25			2 (6%)
2A > 0.25 (PM localization)			8 (22%)
Total			36

Table S2. Homozygous mutations in the Jain Foundation Dysferlin Registry containing DYSF^{PMMs} selected for this study, related to Figure 2. List of 36 DYSF^{PMMs} that exist among 90 of the 327 patients carrying the 113 DYSF^{PMMs} selected for this study. 87 individuals carry a single homozygous PMM, 3 patients are homozygous for both I1607T and Y1014C; 1 patient is homozygous for both R1331L and R253W; in all four cases one of the variants has 2A-expression values >0.25 and the other <0.25. DYSF^{R2042C} is not seen at the PM by ICC assay.

Table S3: Pathogenicity Evidence for DYSF^{PMMs} > 0.25 in 2A-assay

DYSF Missense Mutation	Evidence of Non-Pathogenicity						Evidence of Pathogenicity
	Seen in Patients with Two Other Known Pathogenic DYSF Variants	Seen in Patients in Combination with Variants Predicted to be Pathogenic by 2A-assay	Patient Confirmed with Another MD	Patients Have Carrier or Normal Dysferlin Protein Levels	Altered Splicing	ClinVar Calls Variant Benign	
L7P						X	
W46R							
P134L		X					
A170E						X	
V374L	X						
M451V				X			
E457K						X	
R468C				X			
M626T		X					
T702M	X						
S721T					X		
P731R							X
R803H				X			
I834V						X	
P839L	X						
T881P					X		
T897M		X					
T937I							
M968L				X			
R1022Q			X				
R1022W							
V1119M				X			
G1149R	X						
D1163N			X				
I1208M				X			
I1284T				X			
I1298V	X						
Q1323E			X				
R1342W		X					
N1351S				X			
P1400R		X					
R1581H		X					
K1598N					X		
R1814H							X
M1835V					X		
G2003D							X
A2066T							X
M2073V							X
Total	5	6	3	8	4	4	5
%	13%	16%	8%	21%	11%	11%	13%

Table S3. Supportive evidence for pathogenicity calls on DYSF^{PMMs} where 2A-assay and ICC show PM-localized DYSF, related to Figure 2. The majority of listed DYSF^{PMMs} are found as heterozygous alleles and have evidence of non-pathogenicity. R1814H, G2003D, and P731R are found with other known pathogenic DYSF variants in individuals that show disease range dysferlin protein levels. A2066T and M2073V are each found in trans with pathogenic nonsense mutations in individuals in the registry. No additional pathogenicity evidence is available for L7P, W46R, T937I, or R1022W. ClinVar is the NCBI NIH archive of the relationships among human variations and phenotypes, and has evidence-based calls on pathogenicity.